Clays and Clay Minerals, Vol. 40, No. 6, 682–699, 1992.

SHALE DIAGENESIS: A CASE STUDY FROM THE ALBIAN HARMON MEMBER (PEACE RIVER FORMATION), WESTERN CANADA

J. BLOCH[1] AND I. E. HUTCHEON

Department of Geology and Geophysics, The University of Calgary, Calgary, Alberta, Canada T2N 1N4

Abstract—Shales have often been cited as the source of authigenic material that occurs in coarser grained sediments, but there are few comprehensive studies of diagenesis in shales that rigorously attempt to determine if they are sources for potentially mobile constituents or if they retain those constituents within the shale body. The silicate diagenesis of a Lower Cretaceous marine mudstone, the Harmon Member, was investigated by determining the bulk chemistry, clay mineral compositions and mineral modes using standard analytical techniques and linear programming. Changes in mineralogy are observed in hemipelagic laminated mudstones (LM) that are attributable to diagenesis despite relatively constant bulk compositions. These include authigenic kaolinite formation and illitization of detrital muscovite, K-feldspar and authigenic kaolinite. No diagenetic trends in mineralogy are observed in rapid and episodically deposited transition zone (TZ) sediments because of primary (depositional) mineralogical variability. Diagenetic changes in mineral modes for shales of the Harmon Member are small, suggesting that silicate diagenesis proceeds under relatively "closed system" conditions. The occurrence of authigenic quartz suggests that much of the Si released from the dissolution of quartz and chert is precipitated within the Harmon Member. Al, Ti, and K apparently are conserved. Burial induced increase in temperature is inferred to be the primary control on silicate diagenesis within the Harmon Member.

Key Words—Clay mineralogy, Quantitative shale mineralogy, Silicate diagenesis.

INTRODUCTION

Shales constitute the greatest volume of sedimentary basins, yet their response to burial and diagenesis is poorly understood compared to that of coarser-grained sandstones and carbonates. The source of the material that constitutes the authigenic phases in coarser-grained rocks is difficult to determine, and shales frequently are invoked as sources of silica (Sibley and Blatt, 1976; Land and Dutton, 1978; Boles and Franks, 1979; Land, 1984; Longstaffe, 1984, 1986; Milliken *et al.*, 1989; Tilley and Longstaffe, 1989), CO_2 (Lundegard and Land, 1986), Mg for dolomitization (Mattes and Mountjoy, 1980) and organic acids (Crossey, 1985), among other constituents. Few studies (Perry and Hower, 1970; Hower *et al.*, 1976; Powell *et al.*, 1978; Boles and Franks, 1979; Huggett, 1986; Shaw and Primmer, 1989; Sullivan and McBride, 1991) have examined diagenetic processes in shales to establish whether they are in fact the sources of the components that are attributed to them.

The initial compositional variation in shales must be recognized in order to understand subsequent diagenetic effects. Traditionally, shales have been characterized by their bulk chemistry (Englund and Jorgensen, 1973; Potter *et al.*, 1980), but this approach neglects variations in mineralogy. Mineralogical studies of ancient (Bjørlykke, 1974; Schultz *et al.*, 1980) and Holocene shales (Griffin, 1962; Shaw and Weaver, 1965) have demonstrated variations in mineralogy and the composition of minerals that result from provenance, weathering, transport, and depositional environment. Recent petrologic investigations of shales using image analysis and high-resolution electron beam techniques (Ireland *et al.*, 1983; Huggett and White, 1982; Pye and Krinsley, 1984) indicate that shale mineralogy may be extremely heterogeneous on a pore-size scale (several micrometers). These microscale differences are important in interpreting diagenetic reactions and determining modal mineralogy within shales. Hower *et al.* (1976) demonstrated changes in the mineralogy of specific size fractions of shales with increasing burial depth. These variations may reflect primary composition, and the mineralogy of different size fractions may not be representative of the bulk mineralogy.

Other studies of shale diagenesis have focused on specific mineral reactions, particularly the smectite to illite reaction, and generally have not considered bulk chemistry or modal mineralogy (Schultz, 1978; Perry and Hower, 1970; Foscolos *et al.*, 1976; Pollastro, 1985; Burtner and Warner, 1986). Although the classic studies of the Gulf Coast of the United States (Perry and Hower, 1970; Hower *et al.*, 1976; Boles and Franks, 1979) consider a number of different size fractions, the bulk mineralogy is not documented. To recognize the consequences of shale diagenesis, all mineral phases that potentially are involved in reactions should be considered.

It is not always possible to identify directly the effects of diagenesis in shales using standard petrographic

[1] Present address: Geological Survey of Canada, Institute of Sedimentary and Petroleum Geology, 3303 33rd St. N.W., Calgary, Alberta, Canada T2L 2A7.

Copyright © 1992, The Clay Minerals Society

https://doi.org/10.1346/CCMN.1992.0400608 Published online by Cambridge University Press

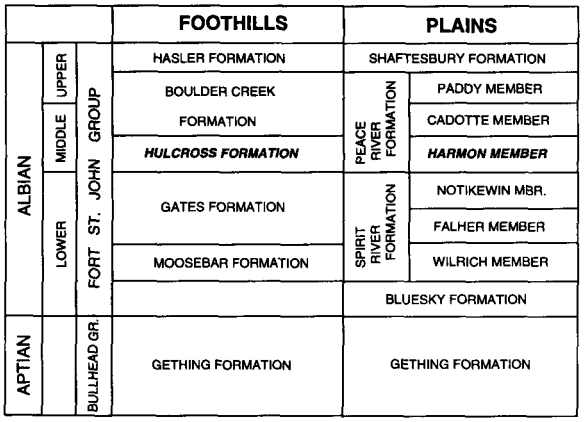

Figure 1. Aptian-Albian stratigraphic nomenclature of the Peace River Foothills (outcrop) and Plains (subsurface), western Canada Sedimentary Basin.

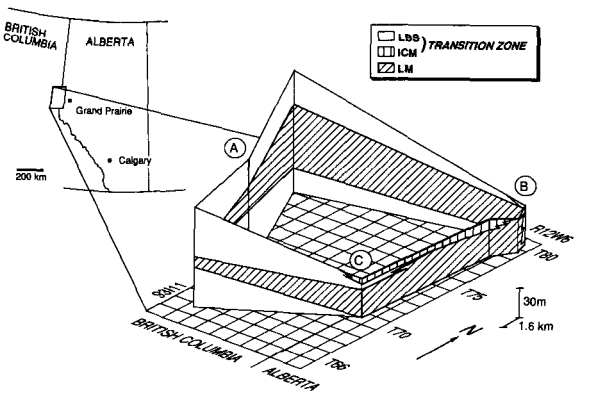

Figure 2. Paleogeographic reconstruction of Harmon Member lithofacies in the study area. No correction for thrust shortening.

techniques because of the fine-grained nature of these rocks and the fact that compaction destroys early formed fabrics, making it difficult to distinguish detrital from authigenic constituents. However, an indirect approach can be pursued that determines 1) modal abundance of minerals, 2) chemical compositions of those minerals, and 3) diagenetic reactions that result in changes in modal abundance and chemical composition.

This study uses a combination of analytical techniques (X-ray diffraction, X-ray fluorescence, carbon and sulphur analyses and Rock-Eval pyrolysis) and linear programming to quantify, as far as is possible, shale modal mineralogy and composition. These data are used to interpret the paragenesis of an illitic marine mudstone unit, the Albian Harmon Member of the Peace River Formation (Figure 1). This unit was chosen because of the availability of drill core and the variable maximum burial depths and degree of diagenesis within a limited areal extent. Detailed studies (Bloch, 1990; Bloch and Krouse, 1992) have presented the stratigraphy and sedimentology as well as the early diagenesis of carbonate and sulphide minerals of the Harmon Member. In this paper, element mobility and the controls on diagenetic reactions in shales are discussed.

GEOLOGICAL BACKGROUND

Depositional setting and lithofacies

The Harmon Member is a wedge of transgressive marine siltstone and mudstone (Figure 2) that was deposited in a restricted basin about 102 Ma under predominantly anoxic to dysaerobic conditions (Stott, 1968; Stelck and Leckie, 1988; Yanagi *et al.*, 1988). We have simplified the classification of Potter *et al.* (1980, Table 1.2) for shales as follows because bed thickness is highly variable: siltstone (>65% silt-sized material), mudstone (33–65% silt-sized material), and claystone (<35% silt-sized material). The remainder of the rock is composed of clay sized material (<4 μm in size).

The Harmon Member contains three lithofacies: laminated to bioturbated siltstone (LBS), laminated mudstone and claystone (LM), and interbedded conglomerate-mudstone (ICM). A paleogeographic reconstruction is illustrated in Figure 2. LBS is the dominant lithology in basin-margin facies (west-southwest of the study area; A in Figure 2); and LM dominates in a distal, deeper-water, hemipelagic depositional environment (northeast; B in Figure 2). ICM occurs mainly as a thin, sheet-like unit that is transitional to the overlying Cadotte Member near to off-shore sands (C in Figure 2). LBS and ICM lithofacies are collectively referred to as transition zone (TZ) sediments.

It is necessary that primary depositional differences in bulk composition of shales be distinguished from changes in mineralogy due to diagenesis. A detailed description of Harmon Member lithofacies (Bloch and Krouse, 1992) is used to assist in the interpretation of depositional *vs* diagenetic variations in mineralogy.

Burial history

The burial history of the Harmon Member in the study area is complex (Kalkreuth and McMechan, 1984, 1988). The time-temperature history, based primarily on stratigraphic reconstruction and vitrinite reflectance data, indicate that the period of maximum burial was reached in the Eocene during the culmination of the Laramide orogeny. Burial history curves (Figure 3) were constructed by linear extrapolation of the time-depth values of Kalkreuth and McMechan (1984, 1988) for the Late Aptian Gething Formation and the latest Albian Boulder Creek Formation, which bracket the Harmon Member (Figure 1). The development of thrusting during Laramide time results in westerly sections (A on Figure 3) being deeply buried and then exhumed

https://doi.org/10.1346/CCMN.1992.0400608 Published online by Cambridge University Press

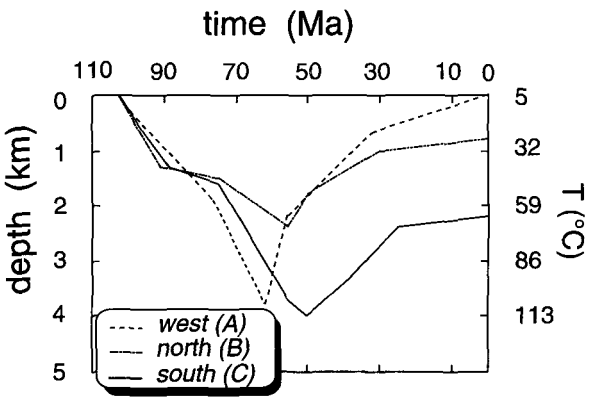

Figure 3. Burial curves for the Harmon Member in the west (A in Figure 2), north (B in Figure 2) and south (C in Figure 2) of the study area.

after erosion. In the north (B on Figure 3), Harmon Member sediments were only buried to about 2 km. In the south (C on Figure 3), sediments were buried to approximately 4 km, the greatest depth observed in the study area. Variation in maximum burial depth results from an increased differential down warping to the southwest of the study area (Hart and Plint, 1990; Leckie *et al.*, 1990). Approximate maximum burial temperatures for the Harmon Member were 110°C in the west (A, Figure 3), 70°C in the north (B, Figure 3) and 115°C in the south (C, Figure 3). This corresponds to depths of 3.8, 4.0, and 2.4 km, respectively. Temperatures are calculated assuming a surface temperature of 5°C and a geothermal gradient of 27°C/km (Kalkreuth and McMechan, 1988). This distribution of maximum burial depths and temperatures suggests that diagenetic grade should increase from north to south-southwest across the study area.

Some measurement of diagenetic maturity is required to assess the effects of diagenesis on mineralogy and bulk composition. If the thermal history has been influenced by tectonic events, such as in the western part of the study area, depth is a problematic indicator of maturity. In terrestrial, organic-rich sediments, vitrinite reflectance (R_o) commonly is used to characterize sediment time-temperature exposure, i.e., as an indicator of thermal and diagenetic maturity. In marine sediments, vitrinite may not be present in sufficient quantities to obtain reliable reflectance characteristics.

The parameter T_{max}, obtained during Rock-Eval pyrolysis, provides an alternative diagenetic indicator. Rock-Eval pyrolysis (Espitalié *et al.*, 1977) provides a temperature of maximum kerogen-hydrocarbon yield (T_{max}) that reflects the maturity of the organic matter within the sample, and this value may be calibrated to vitrinite reflectance (Teichmüller and Durand, 1983). In marine shales T_{max} therefore may proxy as an indicator of thermal maturity.

METHODS

Overview

Shales contain a relatively large proportion of extremely fine-grained material, and direct measurement of the modal amount of minerals by standard techniques, such as point counting, is not possible. Further, the fine grain size does not allow electron microbeam methods to be used for quantitative analysis of mineral composition. It is possible to get accurate bulk chemical compositions, approximate mineral modes, and the range of compositions for clay minerals. With this information, an optimization method based on a system of linear equations (linear programming) is used to determine more accurately both mineral compositions and modes (Pearson, 1978; Hodgson and Dudeney, 1984; Johnson *et al.*, 1985; Slaughter, 1989).

The information required to calculate mineral modes using linear programming includes the bulk chemistry of the rock, the minerals present in the rock, and the composition or range of compositions of those minerals. In this study, the bulk chemistry is determined by X-ray fluorescence (XRF) and combustion techniques for total carbon and sulphur. Organic carbon is a major component (greater than 1 wt. %) in most shales and total organic carbon (TOC) is determined by Rock-Eval pyrolysis. Clay mineral compositions are calculated by linear programming using mineralogical (XRD) and chemical analyses (XRF) of the less than 2 μm fraction. The calculated clay mineral compositions are then used to calculate the mineral modes in the whole-rock samples.

Chemical analyses

Elemental analysis for ten oxides (SiO_2, Al_2O_3, Fe_2O_3, MgO, CaO, MnO, K_2O, Na_2O, TiO_2, P_2O_5) was done by XRF on 51 whole-rock samples and 18 less than 2 μm separates using standard methods (Norrish and Hutton, 1969; Baedecker, 1987). Two clay mineral standards, IMT-1 (Silver Hills illite of Hower and Mowatt, 1966) and Fithian illite (Weaver and Pollard, 1973), were also analyzed by XRF. Analytical precision on replicate samples is less than 0.9 wt. % for SiO_2, 0.5 wt. % for Na_2O, 0.2 wt. % for Al_2O_3 and 0.1 wt. % for the other elements. Loss on ignition (LOI) was determined by combustion and precision is better than 0.7 wt. %.

Total carbon was determined by induction-furnace combustion and thermal conductivity detector. Total sulphur was determined by combustion and infra-red detector. These methods are fully described in Baedecker (1987). Analytical precision, as determined from standards and up to three replicate sample analyses, is better than 0.2 wt. % for carbon abundances up to 8 wt. % and 0.05 wt. % sulphur up to 10 wt. % total sulphur.

TOC analysis was done by Rock-Eval pyrolysis (Es-

https://doi.org/10.1346/CCMN.1992.0400608 Published online by Cambridge University Press

pitalié *et al.*, 1977). Analytical precision for TOC, as determined from standard analyses, is better than 0.08 wt. % and the reproducibility of T_{max} values is within 0.5% or approximately 2°C. Total inorganic carbon (TIC) was determined by difference between total carbon and TOC.

Qualitative mineralogy

The mineralogy of 23 transition zone (TZ) and 28 laminated mudstone and claystone (LM) whole-rock samples was determined by XRD on non-oriented powder mounts using FeKα radiation. Operating conditions were 40 kV, 20 mA, scanning speed of 40 s/°2θ, from 2 to 75 °2θ.

Additional mineralogical data were acquired by backscattered-electron microscopy (BSEM) of polished, epoxy-impregnated, carbon-coated samples. BSEM was done on a Cambridge 250 scanning electron microscope equipped with a KE 4 kV-threshold annular solid-state detector. Operating conditions were 20 kV with 0° tilt. Qualitative analysis for mineral identification was done with a Kevex-7000 energy dispersive X-ray analyzer (EDX).

Clay mineralogy

Clay minerals were characterized by XRD on 48 smeared, oriented less than 2 μm separates using Fe-filtered, CoKα radiation generated at 40 kV and 30 mA. The scanning speed was 1 °2θ/50 s from 4 to 40 °2θ. Samples were run at a relative humidity of approximately 40%, glycerol saturated at 60°C for 8 hours, and heated to 550°C. Pretreatments included the removal of organic matter with a 6% NaClO solution and the addition of Na-metaphosphate to prevent flocculation.

The amount of expandable layers in illite was determined by the method of Srodon (1984). Illite polytypes were determined on 18 non-oriented <2 μm samples using the method of Maxwell and Hower (1967). This method is semi-quantitative and cannot detect illite-2 M abundances lower than about 25%.

Calculation of clay mineral compositions

Clay minerals are a major component of shales and, therefore, their composition must be known as accurately as possible to determine quantitative mineral modes from bulk chemistry. In the Harmon Member, a less than 2 μm separate provides a mineral assemblage with a limited number of phases (less than five). These include illite, kaolinite, chamosite and quartz with rare potassium feldspar. With a chemical analysis of this fraction, accurate clay mineral compositions can be determined by linear programming.

Equations that relate clay mineral composition, mineral mode and the chemical compositions of individual silicate minerals are cast as inequalities and solved simultaneously. The possible solutions to the entire set of linear inequalities can be optimized by minimizing residual values (Slaughter, 1989) to obtain the mode and the compositions of minerals because the mode and the composition of each mineral (which are less well known) must be consistent with the bulk composition which is known to a greater degree of accuracy.

The general case is:

$$a_i x + b_i y + c_i z < 100k_i \quad (1)$$

where a_i, b_i, and c_i are the weight percentages of oxide "i" in minerals x, y and z, and k_i is the abundance of oxide "i" in the sample. The occurrence of amorphous species requires special constraints. If the amorphous species have a different stoichiometry than the corresponding crystalline species, an inequality is required to apportion accurately the oxide compositions among amorphous and crystalline species. This is the type of contraint used for the oxides Al_2O_3, Fe_2O_3, MgO and K_2O. The residuals (the amount of oxide components "left over" after the calculation) are minimized and generally approach zero for all oxides except Al_2O_3 and Fe_2O_3. Residual Al_2O_3 and Fe_2O_3 are considered to represent small amounts (less than 1 wt. %) of amorphous Fe- and Al-oxyhydroxides that are commonly present in shales, particularly in the fine size fraction.

Amorphous silica, if present, has the same stoichiometry as crystalline silica (quartz) and can be included in the total calculated for quartz. The sum of SiO_2 in all silica-bearing minerals, therefore, equals the silica content measured by XRF. The equation for SiO_2 is therefore cast as an equality:

$$a_i x + b_i y + c_i z = 100k_{SiO_2} \quad (2)$$

where a_i, b_i, c_i, x, y, and z are defined as above and k_{SiO_2} = the wt. % in SiO_2 in the sample.

Additional constraints are provided by published chemical and XRD data that limit the range of element ratios or abundances for the compositions of illite and chlorite. These include the SiO_2/Al_2O_3 and K_2O content of illite (Hower and Mowatt, 1966; Weaver and Pollard, 1973), the FeO and MgO content of chamosite (Foster, 1962; Petruk, 1964; Weaver and Pollard, 1973), and a range of oxide sums for both clay minerals (Weaver and Pollard, 1973). The composition of quartz, potassium feldspar, and kaolinite are assumed ideal SiO_2, $KAlSi_3O_8$ and $Al_2Si_2O_5(OH)_4$, respectively. The clay mineral compositions are then used in the calculation of whole-rock mineral modes. Examples of linear programming calculations are given in Bloch (1989).

Calculation of whole-rock mineral modes

The bulk chemistry of a sample represents a mixture of minerals including silicates, sulphide and carbonates. Sulphide and carbonate mineral abundances may be determined from the sulphur and inorganic carbon present in a given sample.

https://doi.org/10.1346/CCMN.1992.0400608 Published online by Cambridge University Press

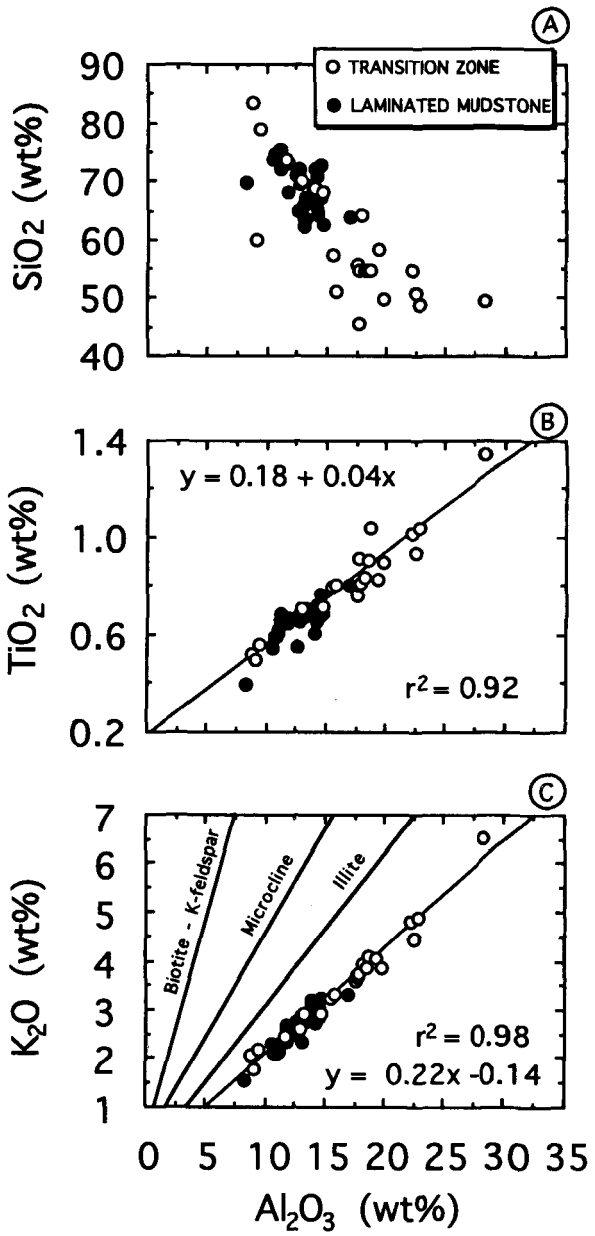

Figure 4. Diagnostic oxide plots for laminated mudstones (LM) and transition zone (TZ) sediments. Lines labeled biotite-K-feldspar, microcline and illite (C) represent the K/Al value for those minerals.

Pyrite is the only sulphur-bearing mineral detected in the Harmon Member. All sulphur is, therefore, assigned to pyrite and the stoichiometric proportion of iron (0.87 wt. % of sulphur; Gautier, 1986) is added to the weight of sulphur to give the abundance of pyrite. Similarly, all P_2O_5 is assigned to an ideal apatite, $Ca_5(PO_4)_3OH$ and a stoichiometric amount of CaO is added to give the abundance of apatite. All TiO_2 is assigned to anatase. The bulk analysis is adjusted by subtracting the amount of each oxide used in the non-silicate minerals.

Carbonate minerals in the Harmon Member generally are disseminated and very fine-grained (Bloch, 1990). Siderite is the dominant carbonate mineral, but most samples contain a mixture of siderite and dolomite with minor calcite or ferroan calcite. To account for the presence of carbonate minerals, CaO, MgO, and FeO are assigned to the TIC content to estimate the components $CaCO_3$, $MgCO_3$, and $FeCO_3$. The presence of specific carbonate minerals is confirmed by petrographic and/or XRD data. This approach adequately accounts for the inorganic carbon present in the rocks but does not describe accurately carbonate mineral composition when more than one carbonate mineral is present.

The remaining oxide abundances are used to calculate the silicate mineral abundances using linear programming, similar to the method described above. In the whole-rock calculations, however, the a_i, b_i and c_i terms of Eqs. (1) and (2) are not variables, and only the mineral abundances—the x, y and z terms—are calculated.

In addition to SiO_2, Al_2O_3, Fe_2O_3, MgO and K_2O, equations for Na_2O and CaO are used when plagioclase is present. Summing the sodium and calcium components gives a plagioclase composition when a single phase of plagioclase is present. The composition of muscovite and annite are assumed ideal $KAl_3Si_3O_{10}(OH)_2$ and $KFe_3AlSi_3O_{10}(OH)_2$, respectively.

The sum of the silicate minerals ($\Sigma_{silicates}$) is assumed to be less than or equal to 100% minus the total of the non-silicates ($\Sigma_{non\text{-}silicates}$) and is expressed as

$$100 - \Sigma_{non\text{-}silicates} \geq \Sigma_{silicates} > m \qquad (3)$$

where m = a minimum value, generally 3 wt. % less than the $100 - \Sigma_{non\text{-}silicates}$ term. This allows for error introduced by compositional variability of the component minerals and the possible presence of small amounts (generally less than 3 wt. %) of amorphous oxides of iron and aluminum and undetected minerals. Eq. (3) provides an additional constraint without adding an unknown phase. The amount of each mineral in a sample may be estimated from XRD and petrographic data. The estimated abundance of each mineral can be cast as a range of allowed values in the linear programming array providing additional constraints.

To test the validity of the method and the accuracy of the results, the chemistry of four clay mixtures comprising analytical standards was determined and the compositions and modes calculated. These mixtures contain variable amounts of purified (less than 2 μm) Upton, Wyoming, smectite (Ross and Hendricks, 1945); Silver Hills illite (Hower and Mowatt, 1966); Chester, Vermont, clinochlore (Foster, 1962); and Macon,

https://doi.org/10.1346/CCMN.1992.0400608 Published online by Cambridge University Press

Georgia, kaolinite (Weaver and Pollard, 1973). The Silver Hills illite contains on average 7.2 wt. % quartz.

RESULTS

Bulk chemistry

LM sediments are more homogeneous in composition than TZ sediments, as shown by the oxide plots in Figure 4 and oxide data in Table 1. Si shows an inverse correlation with Al (Figure 4A), while Ti and K show a high degree of correlation with Al (Figures 4B and 4C, respectively). Clay-mineral-separate oxide abundance from XRF and Rock-Eval, total carbon, and sulphur data are given in Bloch (1989). Elemental whole-rock compositions are given in Table 1.

Qualitative mineralogy

Bulk XRD indicates that the Harmon Member is composed largely of quartz, illite, kaolinite, chlorite, and K-feldspar. BSEM shows that the detrital, non-clay minerals are dominantly quartz and chert grains with subordinate K-feldspar and minor muscovite, chlorite, biotite and rare volcanic rock fragments (Figures 5a–5c). Chert is distinguished from quartz by the microporosity present within grains (Figure 5c). Accessory minerals, identified petrographically, include, in order of decreasing abundance, rutile, apatite, zircon, and sphene. The matrix is composed primarily of micrometer to sub-micrometer size clay particles, and individual phases could not be identified petrographically. EDX analysis of the matrix suggests that it is composed largely of a K-bearing aluminosilicate, most likely illite, with variable amounts of Si, Fe, Mg, and Ti.

Authigenic silicate phases include kaolinite, illite, quartz, and minor chlorite. Authigenic kaolinite forms from the breakdown of detrital micas and as a pore-filling cement (Figure 5d). Kaolinite cement comprises blocky, euhedral kaolin booklets that occlude between 10% and 30% porosity in silt laminations (Figures 5d–5f). The cement fabric shows no evidence of compaction. Authigenic illite may replace detrital K-feldspar (Figure 6a) and authigenic kaolinite; it occurs as well as a neoformed fibrous cement (Figures 6b and 6e). Authigenic illite also replaces authigenic kaolinite (Figure 7a).

While K-feldspar commonly is replaced by illite, it may also be well-preserved (Figures 5a, 5b and 6c). K-feldspar-bearing, silt-sized volcanic rock fragments and discrete detrital K-feldspar grains frequently exhibit little or no evidence of alteration (Figure 5a).

Authigenic quartz is observed as euhedral grains, generally less than 5 μm in size, disseminated in the clay matrix (Figures 6d and 6e) and as overgrowths. Quartz overgrowths are recognized by euhedral grain terminations (Figure 6a) and triple junctions (Figure 6c) and occur predominantly in siltstone or silty mudstone (Figure 5d). Authigenic quartz is also seen in voids created by the mechanical deformation of detrital micas (Figure 6f).

Quartz and chert dissolution textures are pervasive in siltstones and mudstones. Quartz and chert grains show tangential and concavo-convex contacts (Figure 5d), dissolution embayments (Figures 5c and 5f), and intensely dissolved grain margins in contact with illitic matrix (Figure 6f).

It is not clear how much of the chlorite in the Harmon Member is authigenic. Authigenic chlorite is interpreted to form from the alteration of detrital biotite (Figure 7b). However, this is a commonly observed weathering reaction of biotite; therefore, some chlorite formation may have occurred before deposition.

Clay mineralogy

The clay-sized minerals, as determined from the less than 2 μm fraction, are predominantly illite with appreciable kaolinite, quartz, and chamosite. The presence of chamosite is determined by the increased intensity of even-ordered (002, 004) reflections and the occurrence of 1.40 and 0.71 nm peaks after heating to 550°C. The iron-rich composition of chlorite is also apparent from EDX analysis. The expandable component in illite is less than 5%, with the exception of two samples that have 5–10% expandable layers (Figure 8a). The percent 2M-illite polytype ranges from 0% (in 11 samples) up to 60% (Figure 8b). No discrete smecite was identified in the clay separates analyzed.

Clay mineral compositions

The calculated compositions for Harmon Member illite and chlorite are given in Tables 2 and 3, respectively. Illite compositions are shown in Figure 9 and chlorite compositions in Figure 10. A comparison of the calculated compositions for Fithian and Silver Hills illite with published analyses are given in Table 2. The range of calculated compositions (calculation error) is expressed as a compositional envelope about the structural composition of IMT-1 in Figure 9. Contributions to error include analytical uncertainty (Bloch, 1989), the range of possible solutions to the set of linear inequalities, and the possibility of extensive contamination by amorphous oxides of Si, Al, and Fe.

Harmon Member illite is heterogeneous in composition (Figure 9), showing a range of tetrahedral Al (Al^{IV}) substitution between 0.05 and 0.6 and variable Fe and K contents (Table 1). The high total interlayer charge values, greater than 0.6, are consistent with the absence, or very low percentage, of expandable component (Figure 8a). The illite compositional heterogeneity (Figure 8b) most likely reflects the mixture of detrital and authigenic components, calculation uncertainty (see below), and some contamination from Al- and Fe-oxides; and it must be considered that in-

https://doi.org/10.1346/CCMN.1992.0400608 Published online by Cambridge University Press

Table 1. Whole-rock oxide abundances for laminated mudstone (LM) and transition zone sediments (TZ).

Sample no.	SiO_2	Al_2O_3	Fe_2O_3	MgO	CaO	Na_2O	K_2O	TiO_2	P_2O_5	MnO	Sulphur	LOI	Total
Laminated mudstone													
112501	62.36	13.12	5.74	1.04	0.52	0.48	2.315	0.669	0.233	0.02	5.10	10.00	101.57
112506	69.50	12.72	3.60	1.25	0.58	0.54	2.675	0.654	0.222	0.02	1.71	7.67	101.14
112511	64.12	14.22	4.35	1.27	0.44	0.57	3.111	0.656	0.205	0.02	2.90	8.96	100.81
112512	66.67	13.84	3.58	1.43	0.51	0.60	3.115	0.681	0.227	0.02	1.56	7.77	99.98
112515	68.46	13.92	2.81	1.52	0.66	0.54	3.190	0.711	0.235	0.02	0.00	6.92	98.99
062130	68.11	11.88	3.52	1.03	0.48	0.00	2.599	0.645	0.206	0.01	1.60	8.02	98.10
062131	65.83	13.10	4.09	1.19	0.43	0.00	2.886	0.669	0.212	0.01	2.40	8.84	99.66
062132	63.64	13.18	4.48	1.16	0.42	0.00	2.871	0.668	0.204	0.02	2.40	9.52	98.55
011222	67.14	13.30	4.25	1.18	0.49	0.35	2.732	0.705	0.255	0.02	2.20	7.77	100.38
011223	67.21	14.48	4.31	1.21	0.40	0.54	2.835	0.681	0.220	0.01	2.27	7.60	101.77
011224	70.73	12.82	3.25	1.27	0.55	0.62	2.667	0.685	0.226	0.01	1.41	6.72	100.97
011226	72.14	11.23	3.93	0.97	0.46	0.74	2.312	0.666	0.202	0.02	2.23	6.12	101.02
011228	71.89	14.09	3.28	1.29	0.49	2.67	2.913	0.679	0.225	0.01	1.33	6.29	105.16
011230	65.02	14.30	4.49	1.32	0.47	0.33	2.973	0.673	0.215	0.02	2.32	8.61	100.74
100311	73.59	10.94	3.89	0.95	0.40	0.48	2.229	0.593	0.220	0.01	1.80	5.57	100.66
100313	70.07	12.88	3.49	1.00	0.49	0.52	2.597	0.709	0.209	0.01	1.48	7.11	100.57
100315	68.26	14.68	3.95	1.42	0.50	0.80	2.940	0.717	0.219	0.01	1.77	6.81	102.07
102002	63.88	16.92	4.26	1.14	0.46	0.84	3.317	0.806	0.253	0.02	1.93	7.08	100.89
102003	70.78	14.28	3.15	1.16	0.42	0.54	2.707	0.727	0.221	0.01	1.15	6.30	101.45
102004	72.11	12.71	2.98	1.11	0.46	0.39	2.479	0.680	0.213	0.02	1.03	5.44	99.62
102006	73.15	11.90	2.97	1.07	0.49	0.39	2.339	0.672	0.209	0.01	1.21	5.49	99.91
110103	59.91	9.08	12.08	1.10	1.50	0.38	1.789	0.499	0.287	0.05	2.98	10.91	100.56
110105	70.90	12.50	4.20	1.06	0.43	0.22	2.487	0.667	0.207	0.01	2.11	6.19	100.98
110106	74.18	10.97	3.29	0.92	0.45	0.60	2.086	0.604	0.189	0.02	1.35	5.24	99.89
110108	75.19	10.96	2.74	0.98	0.51	0.37	2.130	0.621	0.196	0.01	1.03	5.29	100.03
110110	75.27	11.12	2.91	1.05	0.58	1.23	2.147	0.686	0.199	0.02	1.11	5.28	101.59
110112	69.47	13.83	3.76	1.47	0.55	0.40	2.756	0.694	0.197	0.01	1.70	6.79	101.64
110114	74.52	10.69	3.12	1.22	0.77	0.26	2.106	0.590	0.183	0.02	1.37	5.80	100.65
Mean	69.07	12.84	4.02	1.17	0.53	0.55	2.62	0.67	0.22	0.02	1.84	7.15	
Range	4.04	1.59	1.68	0.16	0.20	0.48	0.38	0.05	0.02	0.01	0.88	1.50	
Transition zone													
062103	54.80	17.72	5.87	2.51	1.64	0.22	3.675	0.807	0.302	0.05	3.45	10.52	101.57
062107	55.55	17.50	6.45	2.55	1.67	0.05	3.606	0.762	0.204	0.08	0.07	11.46	99.95
062113	64.20	17.90	2.80	2.34	1.27	0.44	3.729	0.811	0.173	0.02	0.04	7.84	101.56
062118	58.17	19.29	3.50	2.38	1.47	0.00	4.053	0.827	0.185	0.04	0.08	9.41	99.40
062123	54.71	18.27	5.65	2.10	1.03	0.11	3.953	0.832	0.276	0.05	0.13	12.48	99.59
062125	63.61	13.34	4.49	1.23	0.40	0.00	2.907	0.706	0.243	0.01	2.84	10.23	100.01
062128	64.84	12.60	3.90	1.18	1.60	0.05	2.717	0.680	1.109	0.01	5.30	7.97	101.95
100706	54.64	22.16	4.07	2.20	0.93	0.00	4.811	1.019	0.236	0.02	1.00	8.63	99.70
100711	73.52	11.73	3.70	1.09	0.56	1.02	2.433	0.644	0.242	0.03	0.49	6.17	101.63
101610	50.87	22.48	6.24	2.23	0.83	1.54	4.458	0.937	0.253	0.03	0.67	9.77	100.31
101614	51.01	15.79	11.53	2.18	1.73	0.51	3.333	0.804	0.365	0.10	0.00	12.85	100.20
011211	57.16	15.45	6.05	1.37	0.42	1.60	3.242	0.796	0.205	0.04	2.61	16.16	105.10
011214	48.91	22.89	6.23	3.07	1.61	0.76	4.886	1.042	0.223	0.03	1.47	10.00	101.11
011217	54.82	18.48	6.97	1.94	0.95	1.57	3.857	0.906	0.295	0.02	3.25	9.55	102.59
011220	54.60	18.67	5.76	2.22	1.30	0.40	4.108	1.042	0.308	0.03	1.16	11.02	100.62
810211	78.82	9.46	2.47	0.91	0.50	0.09	2.159	0.562	0.197	0.01	0.31	4.04	99.52
810213	83.34	8.72	1.95	0.75	0.42	0.24	2.064	0.518	0.211	0.01	0.24	3.43	101.90
810215	73.05	11.77	3.45	1.23	0.56	0.00	2.698	0.674	0.216	0.02	1.07	6.01	100.74
810219	71.07	12.63	3.23	1.60	1.24	1.47	2.770	0.550	0.183	0.02	1.19	6.53	102.48
810222	65.91	14.04	4.32	1.81	1.58	1.17	2.921	0.610	0.191	0.02	0.00	8.68	101.24
810225	73.78	10.53	3.22	1.50	1.41	0.63	2.275	0.545	0.195	0.01	1.64	6.75	102.49
810227	62.46	14.71	3.94	1.80	1.15	0.27	3.227	0.686	0.240	0.02	1.32	9.43	99.25
810228	69.74	8.33	5.44	2.35	2.86	0.10	1.549	0.399	0.161	0.04	2.90	9.21	103.80
Mean	62.59	15.41	4.84	1.85	1.18	0.53	3.28	0.75	0.270	0.03	1.36	9.05	
Range	9.46	4.24	1.99	0.59	0.57	0.56	0.87	0.17	0.190	0.02	1.38	2.80	

dividual analyses represent "bulk" sample compositions. Because polytype determination is possible in only a small number of samples, this mixture of illites generally should be considered an *Ad*-polytype (Austin *et al.*, 1989). These results preclude a meaningful interpretation of illite composition within a diagenetic context, and there is no detectable change in illite composition with diagenetic grade.

https://doi.org/10.1346/CCMN.1992.0400608 Published online by Cambridge University Press

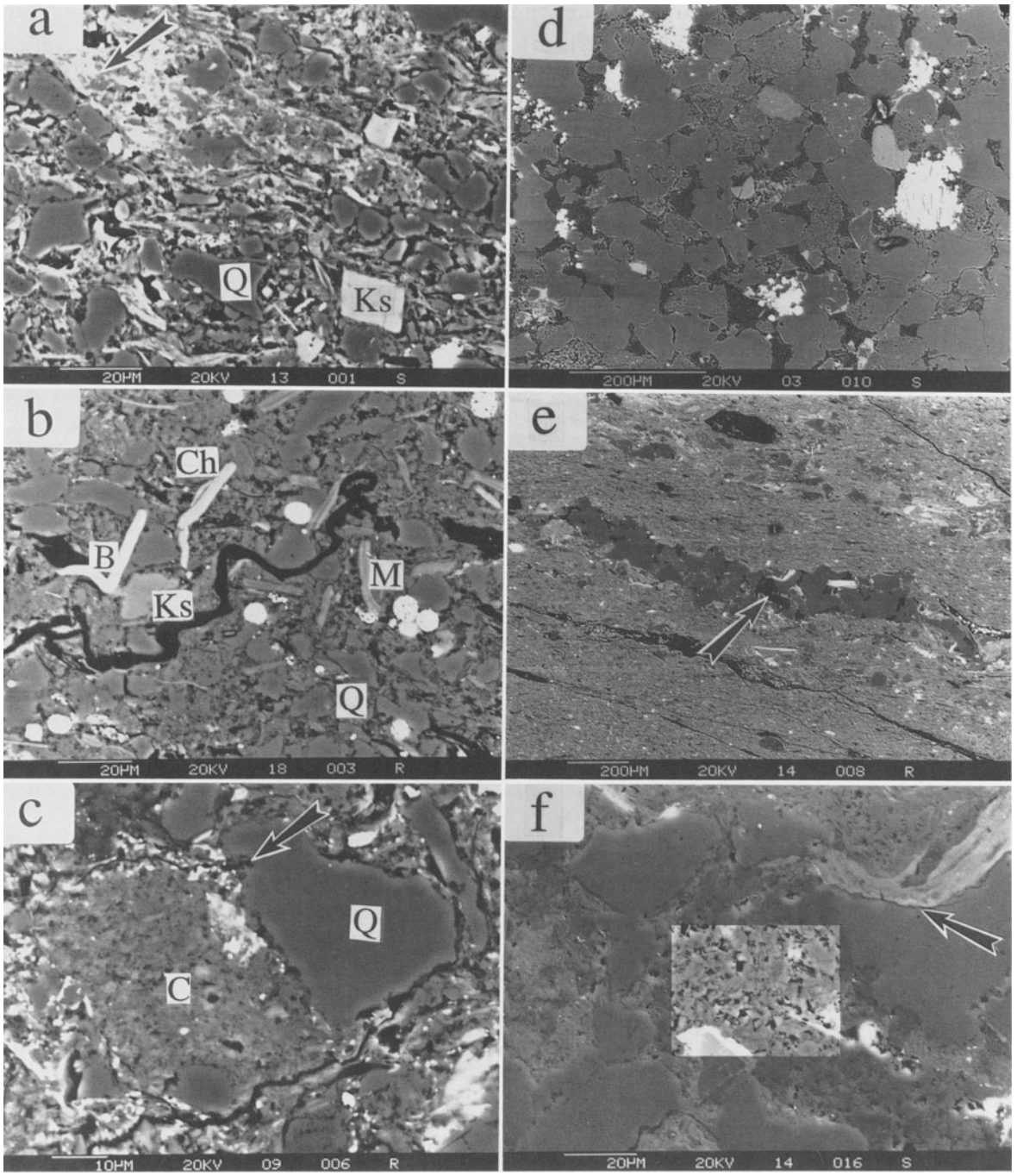

Figure 5. BSE photomicrographs. (a) Well-preserved detrital K-feldspar (Ks) with quartz (Q) and volcanic rock fragments (arrow) that are composed of biotite, K-feldspar and quartz. (b) Typical mudstone containing detrital quartz (Q), K-feldspar (Ks), biotite (B), chlorite (Ch), and muscovite (M). (c) Quartz (Q) and chert (C). Dissolution embayment (arrow) is a common feature of detrital quartz grains. Bright spots in surrounding matrix are pyrite and TiO_2. (d) Siltstone composed of quartz, chert, authigenic pyrite (bright zones), and kaolinite cement (dark zones). Concavo-convex contacts of quartz grains suggest compaction induced dissolution. (e) Silt-starved ripple lamination in claystone with kaolinite cement (arrow). (f) BSE image of kaolinite cement superimposed on a secondary electron image of silt lamination in e. Kaolinite is euhedral and shows no evidence of compaction. Arrow indicates pressure solution of quartz in contact with illitic muscovite.

https://doi.org/10.1346/CCMN.1992.0400608 Published online by Cambridge University Press

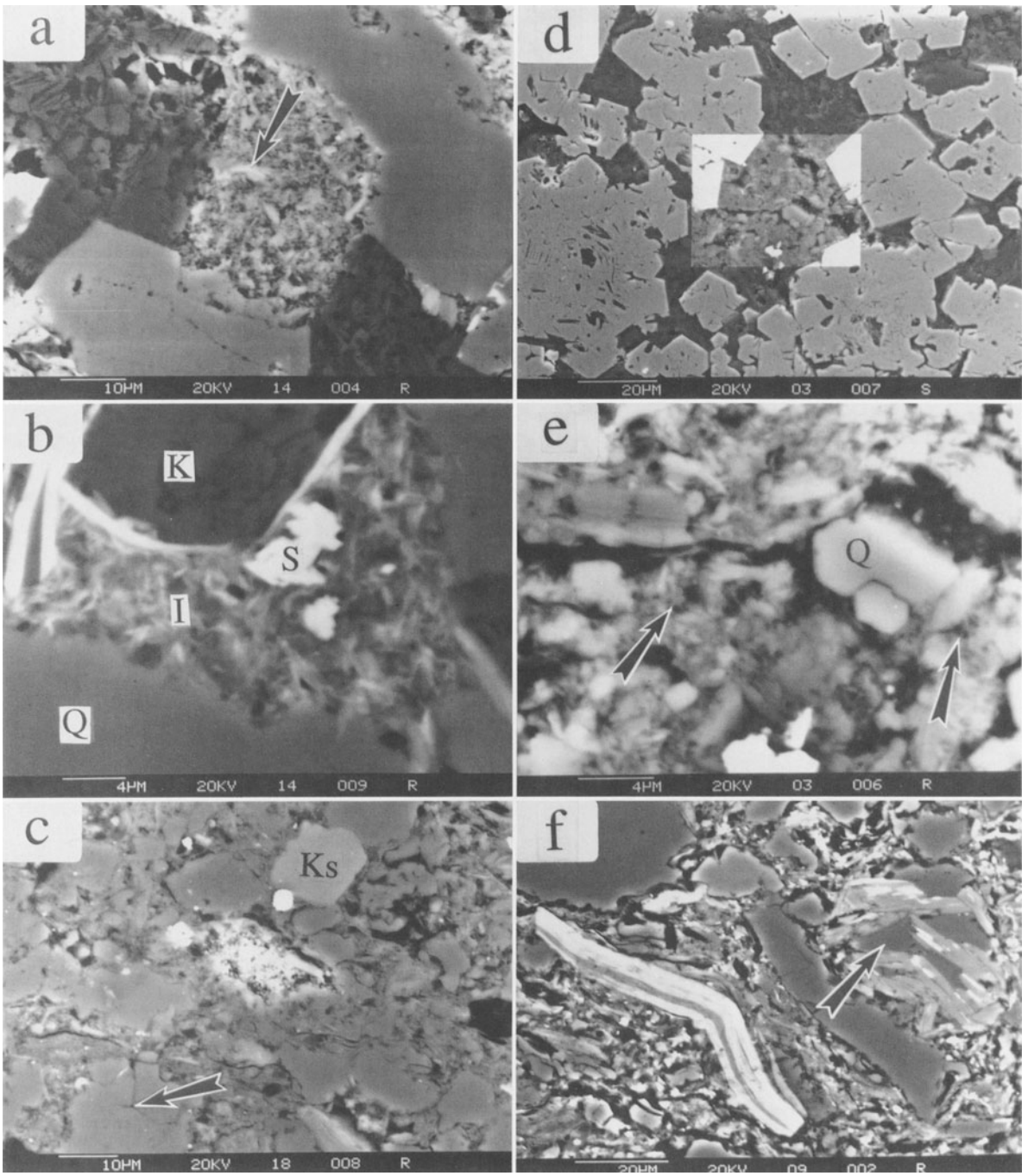

Figure 6. (a) Authigenic illite replaces detrital K-feldspar. Bright zones (arrow) yield EDX K-feldspar compositions. Quartz dissolution has occurred along remnant K-feldspar grain contacts indicating replacement after compaction. Quartz overgrowth (lower left) suggests conservation of SiO_2 within this pore. (b) Authigenic kaolinite (K), illite (I) and siderite (S) in pore adjacent to quartz (Q). (c) Well-preserved K-feldspar (Ks) and quartz triple-junction (arrow). (d) BSE image of authigenic quartz in a non-compacted illitic matrix superimposed on a secondary electron image of authigenic pyrite aggregates that prevent compaction. (e) High-magnification of BSE image in d. Filamentous illite (arrows) appears to bind matrix constituents. Authigenic quartz (Q) is also present. (f) Authigenic quartz (arrow) fills void created in a deformed, almost completely altered biotite. Less altered biotite is at left.

https://doi.org/10.1346/CCMN.1992.0400608 Published online by Cambridge University Press

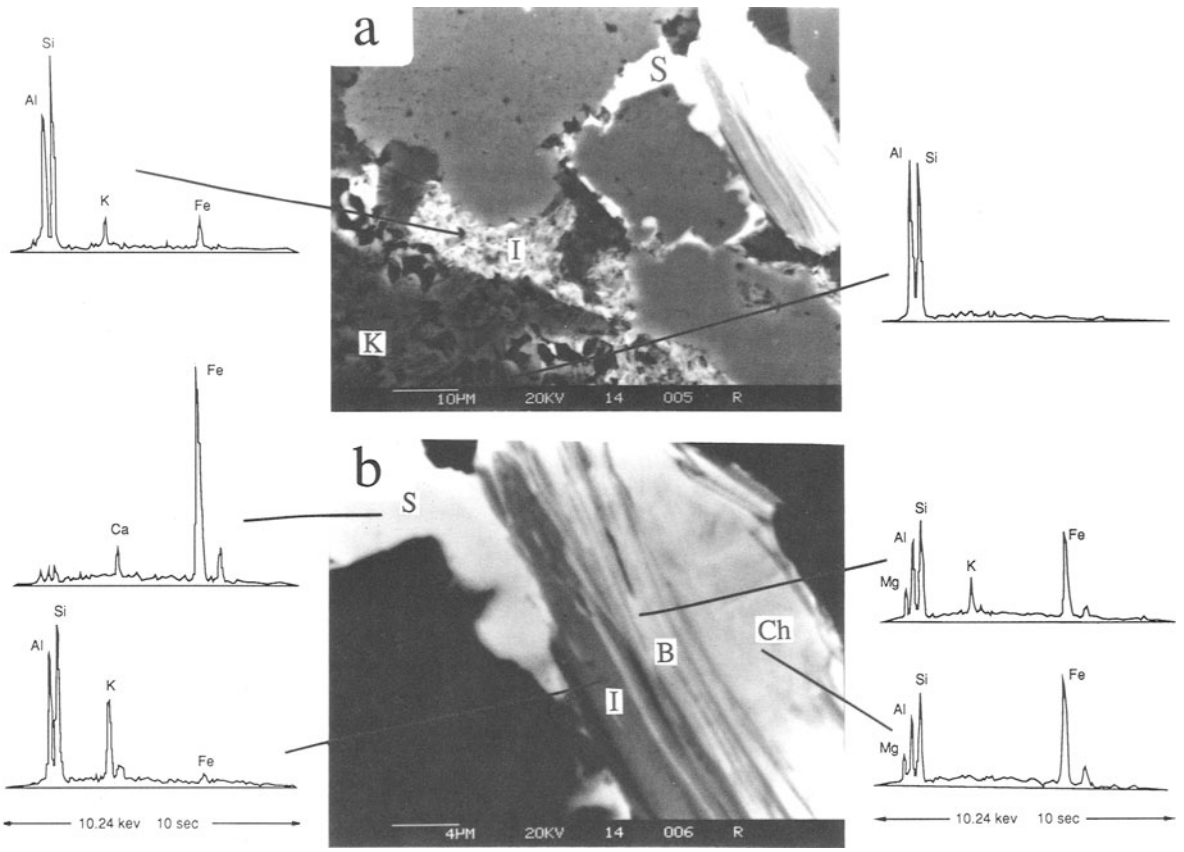

Figure 7. BSE photomicrographs with representative EDX spectra. (a) Authigenic illite (I) replaces kaolinite. Siderite overgrowth (S) on chert grain. (b) Remnant biotite lamellae (B) between illite (I) and authigenic (?) chlorite (Ch). Siderite (S) rim on chert, as in a.

Harmon Member chlorite is an aluminous magnesian-chamosite with low octahedral site occupancy (Figure 10a) that, in composition, resembles authigenic chlorite-1b described by Whittle (1986). The range of calculated compositions is represented by the shaded area about analysis No. 062105, Table 3, Figure 10b. This limited range of compositions is consistent with the observed mechanism of chlorite neo-formation from the breakdown of iron-rich biotite (annite). Furthermore, the chlorite compositions reflect an increase in Si^{IV} relative to annite, suggesting a high activity of silica during chlorite authigenesis. Chlorite compositions are consistent with formation from the breakdown of biotite (Figure 10b), but this is not conclusive evidence for an authigenic origin for most chlorite in the Harmon Member.

Whole rock mineralogy

Standard mixtures. The calculated abundance of minerals using the chemical and XRD data of the standard mineral mixtures is given in Table 4. Five minerals are present in these mixtures. When the composition of all five minerals is known (line 5-5, Table 4), the calculated abundances are within 3 absolute wt. % for all minerals. If the composition of one mineral, in this case illite, is considered to be unknown (lines 5-4 and 4-3, Table 4), the accuracy of the calculated abundances is comparable to the previous case in which all compositions are known. When the composition of two minerals, illite and chlorite, are unknown (lines 5-3 and 4-2, Table 4) the errors in the calculated abundance of all minerals increases substantially—up to about 40% relative error for kaolinite. The composition of smectite must be known to calculate mineral abundances from the chemical data. These results are consistent with the observations of Pearson (1978), who suggested that the presence of significant quantities of clay minerals of increasingly variable composition (illite<chlorite<smectite)—particularly chlorite and smectite or mixed-layer clay—reduces the accuracy of abundance calculations by linear programming. Because the Harmon Member contains no smectite or mixed-layer clay and the compositions of illite and chlorite are accurately calculated, the calculated modal

https://doi.org/10.1346/CCMN.1992.0400608 Published online by Cambridge University Press

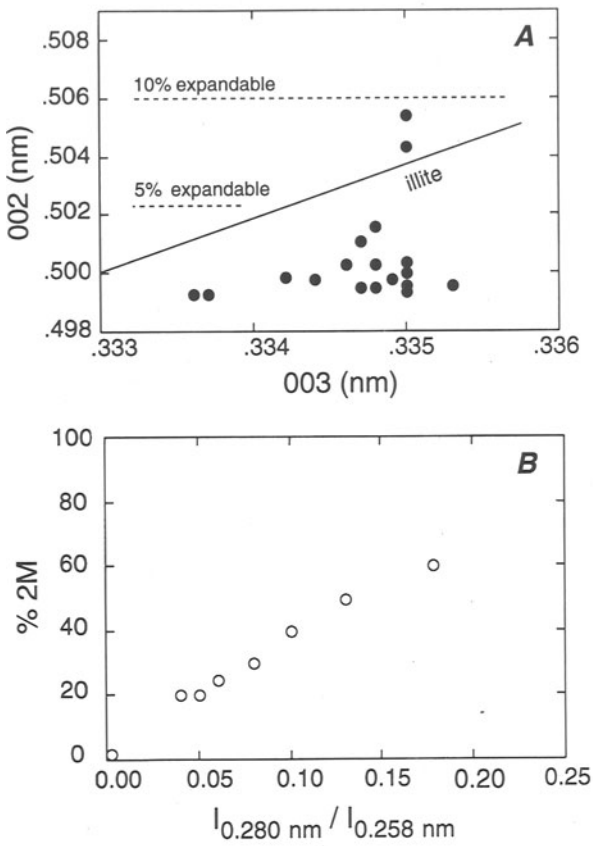

Figure 8. Illite XRD data. (a) Percent expandable layers as determined by the method of Srodon (1984). 002 and 003 d-spacings (nm) are determined from <0.6 μm EG-saturated separates. (b) Percent illite-2 M component in illite by the method of Maxwell and Hower (1967). The data circle at the origin represents 11 samples in which no 2 M polytype was detected.

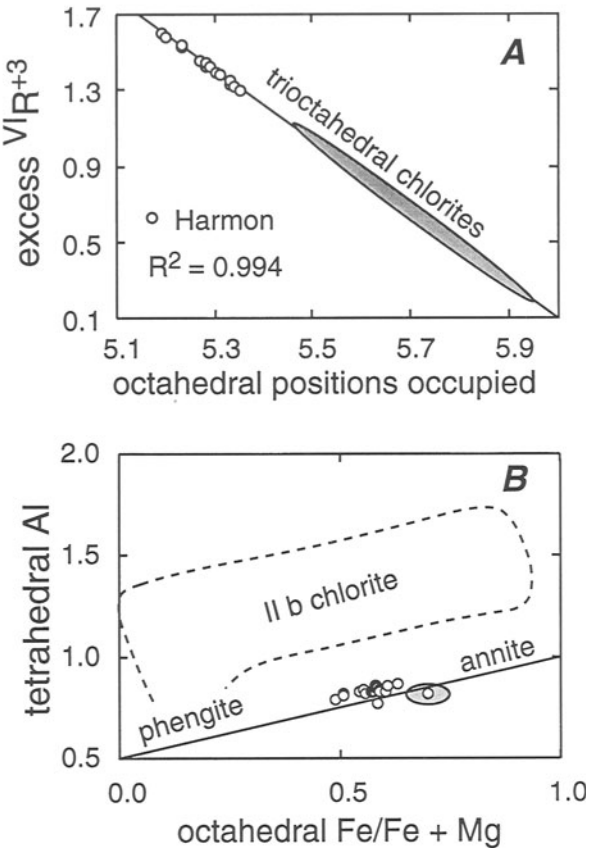

Figure 10. Harmon chlorite compositions calculated from XRF and XRD data. (a) Octahedral site occupancy *vs* octahedral R^{+3} in excess of tetrahedral R^{+3} (excess $^{VI}R^{+3}$). Trioctahedral chlorite data from Foster (1962). (b) Octahedral Fe/Fe + Mg *vs* ^{IV}Al.

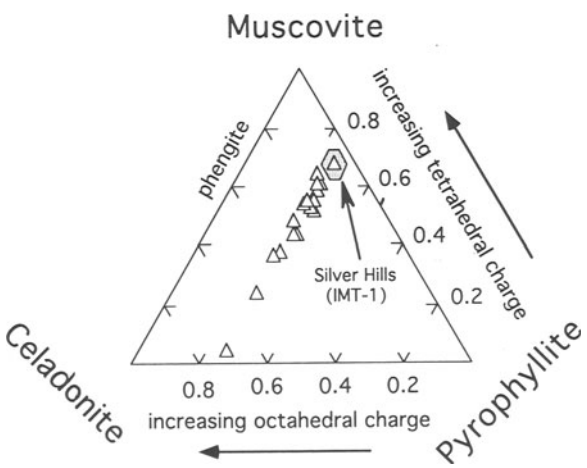

Figure 9. Calculated Harmon Member illite compositions plotted by layer charges, determined from structural formulae (Table 2). Analytical and calculation errors are expressed as compositional variation (shaded area) about the composition of IMT-1 Silver Hills illite.

mineralogy of Harmon Member samples is believed to be accurate within the range presented in Table 4.

Harmon member mineral modes. The mean and range of mineral modes for Harmon Member LM and TZ samples are given in Table 5. Of the six major mineral components, only quartz and illite show significant differences in abundance. These values reflect the effects of depositional processes as well as diagenesis.

DISCUSSION

Paragenesis

The petrographic observations indicate the following paragenetic sequence: kaolinite, illite, quartz, and possibly chlorite. Some kaolinization of micas occurs in association with pyrite formation, indicating a very early genesis. Kaolinite cement occludes 10–30% porosity, also indicative of an early diagenetic origin. Some K-feldspar was preserved during early diagenesis but underwent dissolution and replacement by illite during

https://doi.org/10.1346/CCMN.1992.0400608 Published online by Cambridge University Press

Table 2. Illite compositions and structural formulae calculated from XRF data.

Sample no.	Illite compositions (wt. %)								
	SiO_2	Al_2O_3	K_2O	Fe_2O_3	MgO	Na_2O	CaO	H_2O^1	Total
112504	54.22	19.49	6.52	2.12	0.27	1.13	0.26	14.37	98.38
062105	49.44	23.83	7.14	1.96	2.97	0.95	1.36	11.49	99.14
062121	49.34	23.83	7.15	6.62	2.16	1.04	0.70	8.38	99.22
062130	50.57	24.52	6.28	3.67	1.68	1.44	0.41	10.25	98.81
062132	50.40	22.79	7.05	1.31	0.00	1.45	0.35	14.12	97.47
100706	51.41	26.17	7.60	4.55	2.54	0.87	0.36	7.91	101.41
101614	48.96	24.05	7.00	5.01	1.42	0.90	0.75	11.49	99.57
011214	49.62	25.59	7.37	5.89	2.85	0.89	0.25	8.54	101.00
011220	49.82	23.96	7.33	6.01	2.74	0.94	0.45	9.40	100.65
011223	49.22	23.78	7.33	5.60	2.44	1.09	0.39	10.83	100.69
011230	49.30	23.61	7.32	5.97	2.55	1.27	0.40	11.38	101.80
100305	49.27	26.00	8.69	4.73	2.59	0.91	0.19	8.87	101.25
100315	48.94	23.52	7.51	6.34	2.68	1.06	0.40	10.98	101.43
102002	51.19	25.87	7.39	4.82	2.47	0.99	0.45	9.22	102.39
102006	51.40	26.15	7.61	4.85	2.66	1.18	0.48	8.81	103.14
110103	50.69	22.84	6.75	5.64	0.37	0.97	1.05	12.10	100.41
810211	51.67	26.54	8.38	8.27	2.77	1.09	1.21	8.03	107.96
810223	49.57	23.81	7.14	2.39	0.85	1.04	0.44	13.03	98.27
FITHIAN	49.60	25.50	6.19	6.81	2.33	1.47	0.58	6.90	99.38
FITHIAN[3]	51.74	23.98	5.59	5.56	1.99	0.36	0.97	9.32	99.51
IMT-1	48.68	26.43	8.95	7.39	2.34	0.52	0.29	6.20	100.80
IMT-1[3]	48.60	24.00	8.02	7.20	2.44	0.15	0.35	−8.65	99.41

Sample no.	Structural formulae									
	Tetrahedral		Octahedral				Interlayer			
	Si	Al	Al	Fe^{+3}	Mg	Total	K	Ca	Na^2	Total
112504	3.95	0.05	1.63	0.12	0.03	1.77	0.61	0.04	0.16	0.81
062105	3.56	0.44	1.58	0.11	0.32	2.00	0.66	0.21	0.13	1.00
062121	3.46	0.54	1.43	0.35	0.23	2.01	0.64	0.11	0.14	0.89
062130	3.56	0.44	1.59	0.19	0.18	1.96	0.56	0.06	0.20	0.82
062132	3.76	0.24	1.76	0.07	0.00	1.83	0.67	0.06	0.21	0.94
100706	3.46	0.54	1.53	0.23	0.25	2.02	0.65	0.05	0.11	0.81
101614	3.51	0.49	1.54	0.27	0.15	1.96	0.64	0.11	0.12	0.87
011214	3.39	0.61	1.46	0.30	0.29	2.05	0.64	0.04	0.12	0.80
011220	3.46	0.54	1.43	0.31	0.28	2.02	0.65	0.07	0.13	0.85
011223	3.48	0.52	1.46	0.30	0.26	2.01	0.66	0.06	0.15	0.87
011230	3.47	0.53	1.43	0.32	0.27	2.02	0.66	0.06	0.17	0.89
100305	3.41	0.59	1.52	0.25	0.27	2.04	0.77	0.03	0.12	0.92
100315	3.45	0.55	1.41	0.34	0.28	2.03	0.68	0.06	0.14	0.88
102002	3.46	0.54	1.52	0.24	0.25	2.01	0.64	0.06	0.13	0.83
102006	3.45	0.55	1.51	0.24	0.27	2.02	0.65	0.07	0.15	0.87
110103	3.62	0.38	1.55	0.30	0.04	1.89	0.62	0.16	0.13	0.91
810211	3.35	0.65	1.38	0.40	0.27	2.05	0.69	0.17	0.14	1.00
810223	3.63	0.37	1.68	0.13	0.09	1.91	0.67	0.07	0.15	0.89
FITHIAN	3.39	0.61	1.44	0.35	0.24	2.03	0.54	0.08	0.20	0.82
IMT-1	3.32	0.68	1.44	0.38	0.24	2.06	0.78	0.04	0.07	0.89

[1] Loss on ignition.
[2] Na-saturated.
[3] From Weaver and Pollard, 1973.

subsequent burial. Replacement of K-feldspar by illite occurs after some compaction (Figure 6a), suggesting that K-feldspar dissolution and replacement by illite followed kaolinite precipitation. Sub-micron size fibrous illite (Figure 6e) is also interpreted to have formed after kaolinite cement because of the non-compacted habit and limited pore-space that it occludes. Quartz overgrowths are associated with compaction effects (Figure 6a), and some textures suggest quartz precipitation after significant grain deformation (Figure 6f). These features suggest a relatively late origin for much of the authigenic quartz.

Quartz and chert dissolution textures, however, are common, particularly where grains are in contact with matrix or are matrix supported. Some dissolution textures suggest that compaction induced pressure-solution was the mechanism of quartz dissolution (Figures 5c and 5d). Embayed grains (Figure 7a) show little

https://doi.org/10.1346/CCMN.1992.0400608 Published online by Cambridge University Press

Table 3. Chlorite compositions and structural formulae calculated from XRF data.

	Chlorite compositions (wt. %)					
Sample no.	SiO_2	Al_2O_3	FeO	MgO	H_2O	Total
112504	31.76	25.80	20.76	9.54	12.06	99.92
062105	31.85	27.40	23.30	5.69	12.01	100.25
062121	31.76	26.00	22.44	9.14	12.16	101.50
062130	31.35	25.66	22.06	8.11	11.88	99.06
062132	31.18	26.38	20.93	8.56	11.93	98.98
100706	32.85	27.56	20.05	9.48	12.45	102.39
101614	31.45	25.64	22.02	8.77	11.97	99.85
011214	31.63	26.36	21.14	8.21	11.98	99.32
011220	31.67	26.37	22.81	8.32	12.12	101.29
011223	32.21	26.91	21.63	8.78	12.27	101.80
011230	32.23	26.93	20.81	8.82	12.22	101.01
100305	33.40	28.15	18.37	10.03	12.59	102.54
100315	33.34	28.03	16.98	9.94	12.45	100.74
102002	31.26	25.97	23.64	7.88	11.99	100.74
102006	33.41	28.12	18.42	9.99	12.58	102.52
110103	31.41	24.25	21.27	8.48	11.66	97.07
810211	32.04	26.75	21.63	8.42	12.17	101.01
810223	32.26	26.75	20.23	9.06	12.19	100.49

	Structural formulae						
	Tetrahedral		Octahedral				
Sample no.	Si	Al	Al	Fe	Mg	Total	OH
112504	3.16	0.84	2.19	1.73	1.41	5.33	8.00
062105	3.18	0.82	2.41	1.95	0.85	5.20	8.00
062121	3.14	0.86	2.16	1.85	1.34	5.35	8.00
062130	3.17	0.83	2.22	1.86	1.22	5.31	8.00
062132	3.14	0.86	2.26	1.76	1.28	5.30	8.00
100706	3.17	0.83	2.29	1.61	1.36	5.27	8.00
101614	3.15	0.85	2.18	1.84	1.31	5.33	8.00
011214	3.17	0.83	2.28	1.77	1.23	5.28	8.00
011220	3.14	0.86	2.21	1.89	1.23	5.33	8.00
011223	3.15	0.85	2.25	1.77	1.28	5.30	8.00
011230	3.17	0.83	2.28	1.71	1.29	5.28	8.00
100305	3.18	0.82	2.35	1.46	1.42	5.23	8.00
100315	3.21	0.79	2.40	1.37	1.43	5.19	8.00
102002	3.13	0.87	2.19	1.98	1.17	5.34	8.00
102006	3.19	0.81	2.35	1.47	1.42	5.23	8.00
110103	3.23	0.77	2.17	1.83	1.30	5.30	8.00
810211	3.16	0.84	2.27	1.78	1.24	5.29	8.00
810223	3.18	0.82	2.28	1.66	1.33	5.27	8.00

evidence of compaction effects and suggest a chemical control on silica solubility.

Diagenesis

Effect on mineralogy. Figure 11 shows the mineral abundance for LM and TZ sediments *vs* diagenetic maturity (as indicated by increasing T_{max}). Mineral modes in TZ sediments are generally more variable than LM sediments and show no trends with increasing burial. This suggests that diagenetic processes that result in changes in silicate mineralogy or bulk chemistry are masked by the initial heterogeneity that is induced by the rapid and episodic deposition of these sediments. Similarly, the major constituents quartz and illite in LM sediments show no meaningful diagenetic trends. In this case, the amount of dissolution or mineral authigenesis is small compared to the detrital abundance, and changes in quartz and illite abundances with increasing burial cannot be discerned. The occurrence of authigenic quartz suggests that much of the dissolved Si that is generated during diagenesis is precipitated within the Harmon Member. Chlorite abundances in LM sediments also show no distinct trends, again indicating primary heterogeneity or a high proportion of detrital to authigenic chlorite.

Replacement of kaolinite by illite occurs with increasing diagenesis, and the loss of kaolinite with depth is evident in LM sediments (Figure 11) from a maximum of about 17 wt. % at 1 km present burial depth to 5 wt. % at greater than 2 km present burial depth. Detrital muscovite and K-feldspar are also consumed with increasing diagenesis. The loss of kaolinite, mus-

https://doi.org/10.1346/CCMN.1992.0400608 Published online by Cambridge University Press

Table 4. Comparison of actual and calculated mineral abundances in mixtures of standard clay minerals.

Sample no.	Chlorite	Illite	Kaolinite	Quartz[1]	Smectite
CSM5A actual	6.3	19.7	14.8	1.6	57.7
5-5	7.3	19.7	12.2	1.0	59.9
5-4	7.1	22.9	15.3	3.2	50.5
5-3	9.8	23.1	17.6	4.3	44.3
4-3	6.5	20.1	13.4	1.4	na
4-2	7.2	19.1	13.5	1.6	na
CSM6A actual	10.2	28.0	20.2	2.2	39.4
5-5	11.8	27.4	17.6	1.4	41.8
5-4	9.8	28.5	21.1	2.5	37.7
5-3	15.8	29.4	17.3	4.5	32.9
4-3	9.5	31.3	17.3	2.0	na
4-2	12.9	28.8	15.5	3.1	na
CSM7A actual	14.2	37.2	25.7	2.9	20.0
5-5	16.4	36.5	24.6	2.4	20.1
5-4	13.7	35.7	24.3	1.8	23.9
5-3	23.0	30.4	21.9	3.2	21.4
4-3	12.3	38.6	26.2	2.4	na
4-2	18.3	40.8	16.6	4.1	na
CSM8A actual	2.1	59.5	22.8	4.7	10.9
5-5	1.9	59.3	22.9	6.0	9.8
5-4	5.7	51.0	24.4	5.0	13.7
5-3	7.2	63.2	16.3	4.5	8.3
4-3	3.5	58.0	21.7	5.5	na
4-2	3.9	66.9	13.3	4.8	na

[1] Present as a contaminant in IMT-1 Silver Hills illite.

covite, and K-feldspar with increasing diagenetic maturity indicates that significant changes in mineral modes can occur despite relatively constant bulk composition for LM samples (Tables 1 and 5). The recognition and interpretation of diagenetic processes that occur within shales, therefore, requires detailed mineralogical characterization.

Element mobility and pore fluid compositions. Petrographic observations of TiO_2 in the matrix indicate that Ti precipitates locally when dissolution of Ti-bearing detrital grains occurs, suggesting that Ti is a conservative element. Ti enrichment in weathering profiles also suggests that Ti is immobile under most naturally occurring surfacial (low-temperature) conditions (Brimhall and Dietrich, 1987). Al is also considered to be a conservative element in diagenetic environments (Boles, 1984); however, it has been suggested that Al solubility may be increased by complexation of Al with organic acids (Crossey, 1985). In this study, Al and Ti show a high degree of correlation, suggesting that these elements are conserved during Harmon Member diagenesis. The scatter in the Al-Ti correlation is attributed to multiple sources for Ti that may include non-Al-bearing oxides of Ti (rutile, brookite, ilmenite, and/or leucoxene), sphene, as well as biotite. However, if Ti is considered to be immobile, the strong correlation between Al and Ti suggests that mobilization of Al is not significant.

The K-Al ratio indicates that Harmon Member sediments contain excess Al relative to the dominant Al-bearing phase, illite. It is apparent that, in addition to the observed detrital assemblage, illite − K-feldspar − biotite +/− microcline, an additional non-K-bearing aluminosilicate must have been present in the sediment and was the source of much of the authigenic kaolinite. This precursor phase may initially have been present as detrital kaolinite, plagioclase, and/or amorphous hydroxides of Al.

The K-Al values show a remarkable degree of correlation, suggesting that K, although much more soluble than Ti and Al, is also conserved. The unlikely alternative is that K and Al are lost or gained at a constant proportion in both lithofacies. K is thought to be a mobile constituent during diagenesis (Evans, 1989), and our results are at odds with this observation.

Pore-fluid composition data from modern marine sediments provide constraints on dissolved constituents for ancient shales where no pore-fluid data is available. K concentrations in shallow marine pore fluids of marine shales are generally between 10 and 40 mM/liter (Gieskes *et al.*, 1990; Kastner *et al.*, 1990). This concentration is reduced to less than 5 mM/lilter at depths up to about 500 m (Zachos and Cederburg, 1989) when approximately 50% of the initial sediment volume (pore-fluid) is lost due to compaction and porosity is reduced to about 30% (Hamilton, 1976). Assuming similar pore-fluid and compaction conditions for the Harmon Member, it is inferred that after initial compaction, expelled pore-fluids contained little dissolved K. This is consistent with the observed early formation of kaolinite. While an increase in temperature favors an increase in K solubility, low K concentrations in marine shale pore-fluids relative to sea water may be maintained by clay mineral uptake (Sayles,

Table 5. Summary mineral modes of laminated mudstone (LM) and transition zone sediments (TZ) in wt. %.

	Quartz	Illite	Kaolinite	Chlorite	K-feldspar	Muscovite
Laminated mudstone						
Mean (n = 28)	47	33	7	7.3	2	1
Range	33–60	17–45	0–16	0–14	0–5	0–5
Transition zone						
Mean (n = 23)	35	40	5	6	1	1
Range	10–70	20–65	0–17	0–25	0–4	0–7

https://doi.org/10.1346/CCMN.1992.0400608 Published online by Cambridge University Press

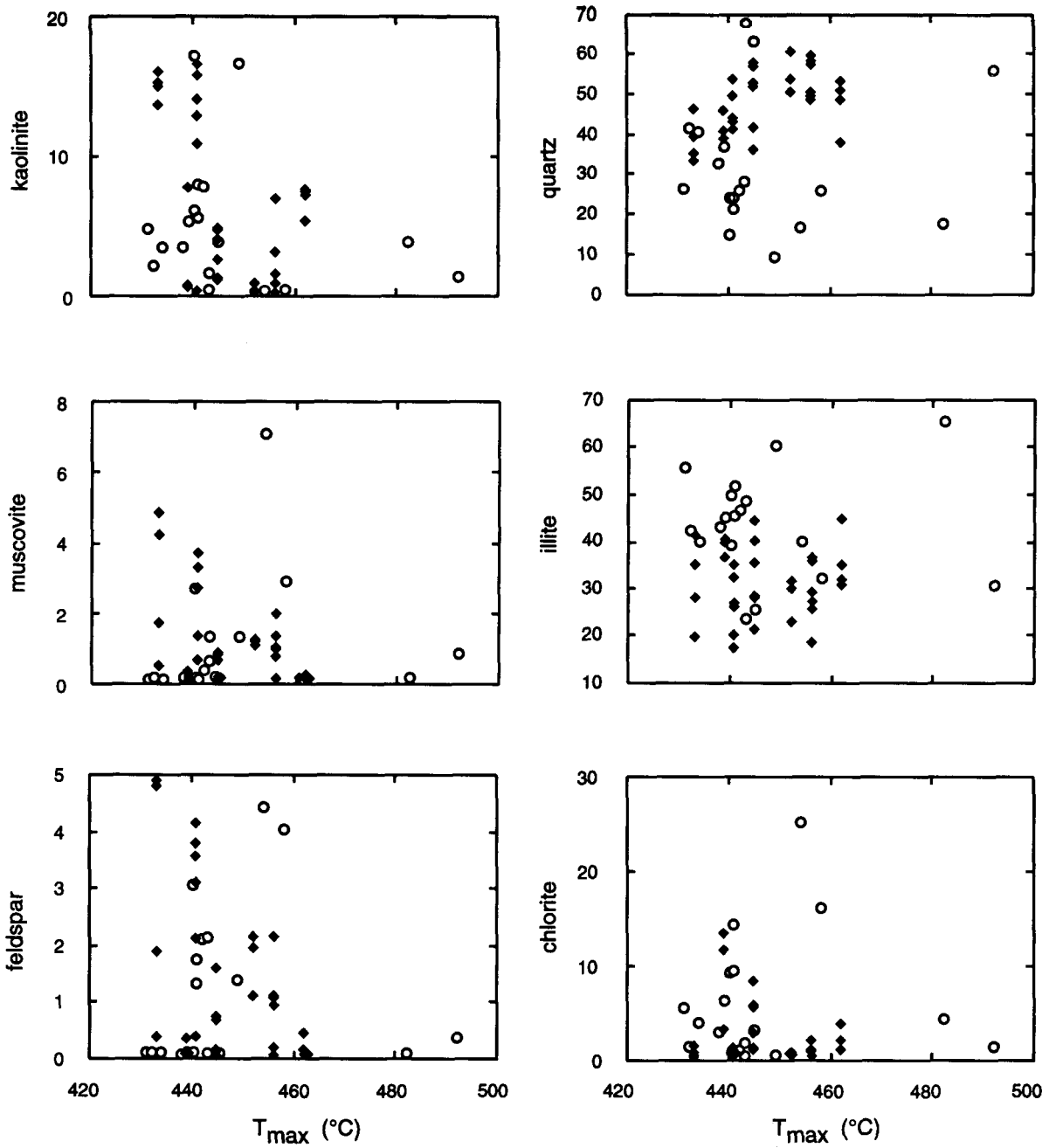

Figure 11. Mineral abundances in weight percent *vs* the pyrolysis maturity indicator, T_{max}. Transition zone samples (open circles) show no trends with increasing diagenetic maturity. The maximum abundances of kaolinite, muscovite, and K-feldspar do show a decrease with increasing T_{max}. Quartz, illite, and chlorite show no trends.

1979). Pore-fluids of the Harmon Member are inferred to have had relatively low dissolved K contents (Figure 12). Subsequent fluid expulsion is slowed by reduced permeability, and normally compacted sediments would be expected to continue dewatering slowly. When fluid-flow rates are low, mineral reactions dominate pore-fluid compositions (Abercrombie, 1988), and the mineralogy of the Harmon Member indicates that low dissolved K concentrations could have been maintained by the mineral assemblage (see below). It follows that little K would be "exported" from this shale unit after the initial stage of compaction.

The mineral assemblage kaolinite, illite (as muscovite with an assumed activity of muscovite in illite of 0.3), and K-feldspar can be represented on a phase diagram (Figure 12) of log aH_4SiO_4 *vs* log $a(K^+/H^+)$

https://doi.org/10.1346/CCMN.1992.0400608 Published online by Cambridge University Press

generated from thermodynamic data (Brown *et al.*, 1988). The paragenesis suggests that the stable assemblage during early diagenesis is kaolinite-illite-K-feldspar; log aH_4SiO_4 must, therefore, be greater than −3.8 or supersaturated with respect to quartz. An upper limit on the aH_4SiO_4 (assuming quartz saturation) can be imposed by the maximum burial temperature. The kaolinite stability field at 25°C constrains log $a(K^+/H^+)$ to less than 5. At neutral pH, this would be equivalent to approximately 10 mM/liter, similar to modern pore-fluids. This inferred range of fluid compositions falls within the illite stability field at maximum burial temperatures, consistent with the observed dissolution of K-feldspar and kaolinite and neoformation of illite.

Controls on diagenetic reactions

At a relatively constant fluid composition with respect to Si and K, the paragenetic sequence of the Harmon Member may be explained by the burial-induced increase in temperature. With increasing temperature, the illite stability field expands (Figure 12) until, at about 125°C, the fluid composition, as inferred from extrapolating modern pore waters and using the burial history of the Harmon Member, is wholly within the illite stability field. This chemography is compatible with the observable changes in mineralogy (Figure 11) dicating that temperature is the primary control on diagenesis within the Harmon Member. Morton (1985) invokes through-going fluid flow in a "punctuated" fashion to explain illite formation from smectite; however, that study considers only the 0.05 μm size fraction. For the Harmon Member, whole-rock compositional data and the observed mineralogy changes provide evidence that K, Al, and Ti essentially are immobile and argue against models that invoke large scale fluid flow through shales.

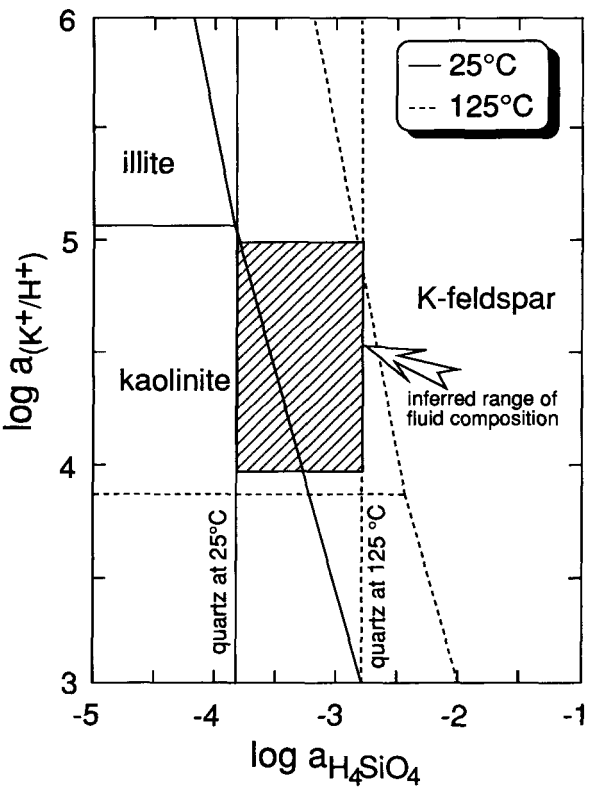

Figure 12. Log a H_4SiO_4 *vs* log a (K+/H+) showing quartz saturation and the stability fields of illite (muscovite with component activity = 0.3), kaolinite, and K-feldspar at 25°C and 125°C. Shaded area represents the range of inferred fluid composition during Harmon Member diagenesis, determined from modern marine shale pore-fluid data.

CONCLUSIONS

The diagenesis of Albian Harmon Member mudstones has been investigated by synthesizing sedimentology, petrographic observations, bulk-chemistry, clay mineralogy, and calculated whole-rock mineral modes using linear programming. Rapidly and episodically deposited transition zone (TZ) sediments are heterogeneous in composition relative to hemipelagic laminated mudstones (LM). The depositionally induced compositional variability of TZ sediments masks diagenetic alteration of modal mineralogy. Within the more homogeneous LM, some diagenetic trends are discerned. The abundances of authigenic kaolinite, detrital muscovite, and K-feldspar decrease with increasing diagenetic maturity. Mineral constituents (quartz, illite, and possibly chlorite) that have a large detrital component show no diagenetic trends because the amount of these minerals consumed or precipitated during diagenesis is small relative to the total abundance. These observations indicate that mineralogical analysis, in addition to bulk chemistry, is necessary for evaluation of diagenetic processes in shales.

The bulk composition of LM sediments remains relatively constant despite changes in the mineralogy suggesting that silicate diagenesis proceeds under relatively "closed-system" conditions. Al, Ti, and K are apparently conserved during diagenesis. Quartz and chert dissolution occur, but quartz overgrowths are common, suggesting that some portion of the dissolved Si is reprecipitated within the shale. Inferred pore-fluid composition and the paragenetic sequence kaolinite-illite-quartz, in association with K-feldspar, indicate that the burial induced increase in temperature is the primary control on diagenesis within the Harmon Member.

ACKNOWLEDGMENTS

This work was supported by Energy, Mines and Resources Canada grants 87-213 and 88-66 and operating grants from the Natural Sciences and Engineering Council of Canada. In addition, we thank Roger Macqueen and Lloyd Snowdon for access to analytical facilities at the Institute of Sedimentary and Petroleum

https://doi.org/10.1346/CCMN.1992.0400608 Published online by Cambridge University Press

Geology. Pat Michael, Al Heinrich, and Jenny Wong assisted with some of the analytical work. The constructive comments of two anonymous *C&CM* reviewers improved the presentation of this material. We are indebted, as ever, to the Dudes of Diagenesis for discussion and support.

REFERENCES

Abercrombie, H. J. (1988) Water-rock interaction during diagenesis and thermal recovery, Cold Lake, Alberta: Ph.D. thesis, The University of Calgary, Calgary, Alberta, 183 pp.

Austin, G. S., Glass, H. D., and Hughes, R. E. (1989) Resolution of the polytype structure of some illitic clay minerals that appear to be 1 Md: *Clays & Clay Minerals* **37,** 128–134.

Baedecker, P. A., ed. (1987) Methods for geochemical analysis: *U.S. Geol. Surv. Bull.* **1770.**

Bjørlykke, K. (1974) Geochemical and mineralogical influence of Ordovician island arcs on epicontinental clastic sedimentation. A study of Lower Paleozoic sedimentation in the Oslo region, Norway: *Sedimentology* **21,** 251–272.

Bloch, J. (1989) Diagenesis and rock-fluid interaction of Cretaceous Harmon Member (Fort St. John Group) mudstones, Alberta and British Columbia: Ph.D. thesis, The University of Calgary, Calgary, Alberta, 165 pp.

Bloch, J. (1990) Stable isotopic composition of authigenic carbonates from the Albian Harmon Member (Peace River Formation): Evidence of early diagenetic processes: *Bull. Can. Pet. Geol.* **38,** 39–52.

Bloch, J. and Krouse, H. R. (1992) Sulfide diagenesis and sedimentation in the Harmon Member, western Canada: *Jour. Sed. Pet.* **62,** 235–249.

Boles, J. R. (1984) Secondary porosity reactions in the Stevens Sandstone, San Joachin Valley, California: in *Clastic Diagenesis,* D. A. McDonald and R. C. Surdam, eds., Amer. Assoc. Pet. Geol. Mem. **37,** 217–234.

Boles, J. R. and Franks, S. G. (1979) Clay diagenesis in Wilcox sandstones of southwest Texas: Implications of smectite diagenesis on sandstone cementation: *Jour. Sed. Pet.* **49,** 55–70.

Brimhall, G. H. and Dietrich, W. E. (1987) Constitutive mass balance relations between chemical composition, volume, density, porosity, and strain in metasomatic hydrochemical systems: Results on weathering and pedogenesis: *Geochim. Cosmochim. Acta* **51,** 567–587.

Brown, T. H., Berman, R. G., and Perkins, E. H. (1988) GEO-CALC: Software package for calculation and display of pressure-temperature-composition phase diagrams using an IBM or compatible personal computer: *Computers and Geosciences* **14,** 279–289.

Burtner, R. L. and Warner, M. A. (1986) Relationship between illite/smectite diagenesis and hydrocarbon generation in Lower Cretaceous Mowry and Skull Creek shales of the Northern Rocky Mountain Area: *Clays & Clay Minerals* **34,** 390–402.

Crossey, L. J. (1985) The origin and role of water-soluble organic compounds in clastic diagenetic systems: Ph.D. thesis, University of Wyoming, Laramie, Wyoming, 134 pp.

Englund, J. O. and Jorgensen, P. (1973) A chemical classification system for argillaceous sediments and factors affecting their composition: *Geol. fören Stockholm Förh.* **95,** 87–97.

Espitalié, J., Laporte, J. L., Madec, M., Marquis, F., Leplat, P., Paulet, J., and Boutefeu, A. (1977) Méthode rapide de caractérisation des roches méres de leur potentiel pétrolier et de leur degré d'évolution: *Rev. de Inst. Francais Pét.* **32,** 23–42.

Evans, I. J. (1989) Geochemical fluxes during shale diagenesis, an example from the Ordovician of Morocco: in *Water-Rock Interaction WRI-6, Proceedings of the 6th Internation Symposium on Water-Rock Interaction, Malvern, 3–8 August 1989,* D. L. Miles, ed., Balkema, Rotterdam, 219–222.

Foscolos, A. E., Powell, T. G., and Gunther, P. R. (1976) The use of clay minerals and inorganic and organic geochemical indicators for evaluating the degree of diagenesis and oil generating potential of shales: *Geochim. Cosmochim. Acta* **40,** 953–966.

Foster, M. D. (1962) Interpretation of the composition and a classification of the chlorites: *U.S. Geol. Surv. Prof. Pap.* **414-A,** 33 pp.

Gautier, D. L. (1986) Cretaceous shales from the western interior of North America: Sulfur/carbon ratios and sulfur-isotope composition: *Geology* **14,** 225–228.

Gieskes, J. M., Blanc, G., Vrolijk, P., Elderfield, H., and Barnes, R. (1990) Interstitial water chemistry—Major constituents: in *Proc. Ocean Drill. Prog., Sci. Results* **110,** J. C. Moore and A. Mascle, eds., 155–177.

Griffin, G. M. (1962) Regional clay-mineral facies—Products of weathering intensity and current distribution in the northeastern Gulf of Mexico: *Geol. Soc. Amer. Bull.* **73,** 737–768.

Hamilton, E. L. (1976) Variations of density and porosity with depth in deep-sea sediments: *Jour. Sed. Pet.* **46,** 280–300.

Hart, B. S. and Plint, A. G. (1990) Upper Cretaceous warping and fault movement on the southern flank of the Peace River Arch, Alberta: *Bull. Can. Pet. Geol.* **38A,** 190–195.

Hodgson, M. and Dudeney, A. W. (1984) Estimation of clay proportions in mixtures by X-ray diffraction and computerized mass balance: *Clays & Clay Minerals* **32,** 19–28.

Hower, J. and Mowatt, T. C. (1966) The mineralogy of illites and mixed-layer illite/montmorillonites: *Amer. Mineral.* **51,** 825–854.

Hower, J., Eslinger, E. V., Hower, M. E., and Perry, E. A. (1976) Mechanism of burial metamorphism of argillaceous sediment—1. Mineralogical and chemical evidence: *Bull. Geol. Soc. Amer.* **87,** 725–737.

Huggett, J. M. (1986) An SEM study of phyllosilicate diagenesis in sandstones and mudstones in the Westphalian Coal Measures using back-scattered electron microscopy: *Clay Min.* **21,** 603–616.

Huggett, J. M. and White, S. H. (1982) High-voltage electron microscopy of authigenic clay minerals in sandstones: *Clays & Clay Minerals* **30,** 232–236.

Ireland, B. J., Curtis, C. D., and Whiteman, J. A. (1983) Compositional variation within some glauconites and illites and implications for their stability and origins: *Sedimentology* **30,** 769–786.

Johnson, L. J., Chu, C. H., and Hussey, G. A. (1985) Quantitative clay mineral analysis using simultaneous linear equations: *Clays & Clay Minerals* **33,** 107–117.

Kalkreuth, W. and McMechan, M. E. (1984) Regional pattern of thermal maturation as determined from coal-rank studies, Rocky Mountain foothills and front ranges north of Grande Cache, Alberta—Implications for petroleum exploration: *Bull. Can. Pet. Geol.* **32,** 249–271.

Kalkreuth, W. and McMechan, M. E. (1988) Burial history and thermal maturity, Rocky Mountain front ranges, foothills, and foreland, east-central British Columbia and adjacent Alberta, Canada: *Amer. Assoc. Pet. Geol. Bull.* **72,** 1395–1410.

Kastner, M., Elderfield, H., Martin, J. B., Suess, E., Kvenvolden, K. A., and Garrison, R. E. (1990) Diagenesis and interstitial-water chemistry at the Peruvian continental margin—major constituents and strontium isotopes: in *Proc.*

https://doi.org/10.1346/CCMN.1992.0400608 Published online by Cambridge University Press

Ocean Drill. Prog., Sci. Results **112,** E. Suess *et al.,* eds., U.S. Government Printing Office, Washington, D.C., 413–417.

Land, L. S. (1984) Frio Sandstone diagenesis, Texas Gulf Coast: A regional isotopic study: in *Clastic Diagenesis,* D. A. McDonald and R. C. Surdam, eds., Amer. Assoc. Pet. Geol. Mem. **37,** 47–62.

Land, L. S. and Dutton, S. P. (1978) Cementation of a Pennsylvanian deltaic sandstone: Isotopic data: *Jour. Sed. Pet.* **48,** 1167–1176.

Leckie, D. A., Kalkreuth, W. D., and Snowdon, L. R. (1988) Results of Rock-Eval/TOC analysis of a core through the Lower Cretaceous: Monkman Pass Area, northeastern British Columbia: *Amer. Assoc. Pet. Geol. Bull.* **72,** 820–838.

Leckie, D. A., Staniland, M. R., and Hayes, B. J. (1990) Regional maps of the Albian Peace River and lower Shaftesbury formations on the Peace River Arch, northwestern Alberta and northeastern British Columbia: *Bull. Can. Pet. Geol.* **38A,** 176–189.

Longstaffe, F. J. (1984) The role of meteoric diagenesis of shallow sandstones: Stable isotope studies of the Milk River aquifer and gas pool, southeastern Alberta: in *Clastic Diagenesis,* D. A. Macdonald and R. C. Surdam, eds., Amer. Assoc. Pet. Geol. Mem. **37,** 81–98.

Longstaffe, F. J. (1986) Oxygen isotope studies of diagenesis in the basal Belly River Sandstone, Pembina I-pool, Alberta: *Jour. Sed. Pet.* **56,** 78–88.

Lundegard, P. D. and Land, L. S. (1986) Carbon dioxide and organic acids: Their role in porosity enhancement and diagenesis, Paleogene of the Texas: *Gulf Coast Soc. Econ. Paleon. Mineral. Spec. Pub.* **38,** 129–146.

Mattes, B. W. and Mountjoy, E. W. (1980) Burial dolomitization of the Upper Miette buildup, Jasper National Park: in *Concepts and Models of Dolomitization,* D. H. Zenger, J. B. Dunham, and R. L. Ethington, eds., *Soc. Econ. Paleon. Mineral. Spec. Pub.* **28,** 259–297.

Maxwell, D. T. and Hower, J. (1967) High-grade diagenesis and low-grade metamorphism of illite in the Precambrian Belt Series: *Amer. Mineral.* **52,** 843–857.

Milliken, K. L., McBride, E. F., and Land, L. S. (1989) Numerical assessment of dissolution *vs* replacement in the subsurface destruction of detrital feldspars, Oligocene Frio Formation, south Texas: *Jour. Sed. Pet.* **59,** 740–757.

Morton, J. P. (1985) Rb-Sr evidence for punctuated illite/smectite diagenesis in the Oligocene Frio Formation, Texas Gulf Coast: *Geol. Soc. Amer. Bull.* **96,** 114–122.

Norrish, K. and Hutton, J. T. (1969) An accurate X-ray spectrographic method for the analysis of a wide range of geological samples: *Geochim. Cosmochim. Acta* **33,** 431–453.

Pearson, M. J. (1978) Quantitative clay mineralogical analyses from the bulk chemistry of sedimentary rocks: *Clays & Clay Minerals* **26,** 423–433.

Perry, E. and Hower, J. (1970) Burial diagenesis in Gulf Coast pelitic sediments: *Clays & Clay Minerals* **18,** 165–177.

Petruk, W. (1964) Determination of the heavy atom content in chlorite by means of the X-ray diffractometer: *Amer. Mineral.* **49,** 61–71.

Pollastro, R. M. (1985) Mineralogical and morphological evidence for the formation of illite at the expense of illite/smectite: *Clays & Clay Minerals* **33,** 265–274.

Potter, P. E., Maynard, J. B., and Pryor, W. A. (1980) *Sedimentology of Shale:* Springer-Verlag, New York, 303 pp.

Powell, T. G., Foscolos, A. E., Gunther, P. R., and Snowdon, L. R. (1978) Diagenesis of organic matter and fine clay minerals: A comparative study: *Geochim. Cosmochim. Acta* **42,** 1181–1197.

Pye, K. and Krinsley, D. H. (1984) Petrographic examination of sedimentary rocks in the SEM using backscattered electron detectors: *Jour. Sed. Pet.* **54,** 877–888.

Ross, C. S. and Hendricks, S. B. (1945) Minerals of the montmorillonite group, their origin and relation to soils and clays: *U.S. Geol. Surv. Prof. Pap.* **205-B,** 23–72.

Sayles, F. L. (1979) The composition and diagenesis of interstitial solutions—1: Fluxes across the seawater-sediment interface in the Atlantic Ocean: *Geochim. Cosmochim. Acta* **43,** 527–545.

Schultz, L. G. (1978) Mixed-layer clay in the Pierre Shale and equivalent rocks, Northern Great Plains Region: *U.S. Geol. Surv. Prof. Pap.* **1064-A,** 28 pp.

Schultz, L. G., Tourtelot, H. A., Gill, J. R., and Boerngen, J. G. (1980) Composition and properties of the Pierre Shale and equivalent rocks, Northern Great Plains region: *U.S. Geol. Surv. Prof. Pap.* **1064-B,** 114 pp.

Shaw, D. B. and Weaver, C. E. (1965) The mineralogical composition of shales: *Jour. Sed. Pet.* **35,** 213–222.

Shaw, H. F. and Primmer, T. J. (1989) Diagenesis in shales from a partly overpressured sequence in the Gulf Coast, Texas, USA: *Mar. Pet. Geol.* **6,** 121–128.

Sibley, D. F. and Blatt, H. (1976) Intergranular pressure solution and cementation of the Tuscarora orthoquartzite: *Jour. Sed. Pet.* **46,** 881–896.

Slaughter, M. (1989) Quantitative determination of clays and other minerals in rocks: in *Quantitative Mineral Analysis of Clays,* D. R. Pevear and F. A. Mumpton, eds., Clay Min. Soc. Work. Lec. **1,** 120–153.

Srodon, J. (1984) X-ray powder diffraction identification of illitic materials: *Clays & Clay Minerals* **32,** 337–349.

Stelck, C. R. and Leckie, D. (1988) Foraminiferal inventory and lithologic description of the Lower Cretaceous (Albian) Hulcross shale, Monkman area, northeastern British Columbia: *Can. Jour. Ear. Sci.* **25,** 793–798.

Stott, D. F. (1968) Lower Cretaceous Bullhead and Fort St. John Groups, between Smoky and Peace rivers, Rocky Mountain foothills, Alberta and British Columbia: *Geol. Surv. Can. Bull.* **152,** 279 pp.

Sullivan, K. B. and McBride, E. F. (1991) Diagenesis of sandstones at shale contacts and diagenetic heterogeneity, Frio Formation, Texas: *Amer. Assoc. Pet. Geol. Bull.* **75,** 121–138.

Teichmüller, M. and Durand, B. (1983) Fluorescence microscopical rank studies on liptinites and vitrinites in peat and coals and comparison with the results of the Rock-Eval pyrolysis: *Inter. Jour. Coal Geol.* **2,** 197–230.

Tilley, B. J. and Longstaffe, F. J. (1989) Diagenesis and isotopic evolution of porewaters in the Alberta Deep Basin: The Falher Member and Cadomin Formation: *Geochim. Cosmochim. Acta* **53,** 2529–2546.

Weaver, C. E. and Pollard, L. D. (1973) *The Chemistry of Clay Minerals: Developments in Sedimentology 15:* Elsevier, New York, 213 pp.

Whittle, C. K. (1986) Comparison of sedimentary chlorite compositions by X-ray diffraction and analytical TEM: *Clay Miner.* **21,** 937–947.

Yanagi, T., Baadsgaard, H., Stelck, C. R., and McDougall, I. (1988) Radiometric dating of a tuff bed in the middle Albian Hulcross Formation at Hudson's Hope, British Columbia: *Can. Jour. Earth Sci.* **25,** 1123–1127.

Zachos, J. C., and Cederburg, T. (1989) Interstitial Water Chemistry: Sites 645, 646, and 647, Baffin Bay and Labrador Sea: in *Proc. Ocean Drill. Prog. Sci. Results* **115,** 171–183.

(Received 3 April 1992; accepted 9 October 1992; Ms. 2207)

https://doi.org/10.1346/CCMN.1992.0400608 Published online by Cambridge University Press